Vacuum 218 (2023) 112621

Contents lists available at ScienceDirect

Vacuum

journal homepage: www.elsevier.com/locate/vacuum

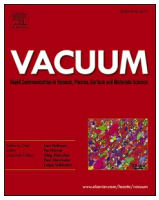

Effects of helium (He) bubbles and annealing on the structural evolution and migration behavior of silver (Ag) implanted into polycrystalline SiC at 350 °C

S.Z. Mtsi [a,*], A. Sohatsky [c], Z.A.Y. Abdalla [a], E.G. Njoroge [a,b], V.A. Skuratov [c,d,e], S.V. Motloung [f], J.B. Malherbe [a], T.T. Hlatshwayo [a]

[a] Physics Department, University of Pretoria, Pretoria, 0002, South Africa
[b] ENGAGE, University of Pretoria, Pretoria, 0002, South Africa
[c] Joint Institute for Nuclear Research, Dubna, Russia
[d] Dubna State University, Dubna, Moscow Region, Russia
[e] National Research Nuclear University MEPhI, Moscow, Russia
[f] School of Physical and Chemical Sciences, North West University (Mahikeng Campus), South Africa

ARTICLE INFO

Handling Editor: Prof. L.G. Hultman

The effects of helium (He) bubbles and annealing on the structural evolution and the migration of silver (Ag) implanted into polycrystalline silicon carbide were investigated. Ag ions of 360 keV were implanted into polycrystalline SiC to a fluence of 2×10^{16} cm^{-2} at 350 °C (Ag-SiC). Some of the implanted samples were then implanted with He ions of 17 keV to a fluence of 1×10^{17} cm^{-2} also at 350 °C (Ag + He-SiC). The Ag-SiC and Ag + He-SiC samples were then annealed at 1100 °C for 5 h. The as-implanted and annealed samples were characterized by Raman spectroscopy, scanning electron microscopy (SEM) and atomic force microscopy (AFM), Rutherford backscattering spectrometry (RBS) and transmission electron microscopy (TEM). Implantation of Ag resulted in the accumulation of defects in SiC without amorphization. Co-implantation of He resulted in the formation of elongated and tiny He bubbles accompanied by the formation of blisters and holes on the surface. Annealing at 1100 °C resulted in some recovery of the SiC crystal structure, indicating that some defects were annealed out in both Ag-SiC and Ag + He-SiC. This was accompanied by the appearance of more holes on the annealed Ag + He-SiC surface and bigger cavities in the co-implanted SiC layer. Some limited migration of implanted Ag accompanied by the formation of Ag precipitates was observed in the as-implanted Ag + He-SiC sample. No migration of Ag was observed in the annealed Ag-SiC samples while migration of Ag towards the surface accompanied by loss was observed in the annealed Ag + He-SiC sample. The migration of Ag in the annealed Ag + He-SiC was also accompanied by the formation of big Ag precipitates trapped in the cavities. Hence, He bubbles assisted the migration of Ag while cavities trapped the Ag in the Ag + He-SiC samples.

1. Introduction

The renewal of fission nuclear reactors as a clean energy source requires a clear demonstration of a complete containment of all radioactive fission products during normal operation and potential accidents. In modern high-temperature gas-cooled reactors (HTGRs) such as a pebble bed modular reactor (PBMR), containment is improved by coating the fuel particle with four chemical vapor deposited (CVD) layers of carbon and silicon carbide (SiC) [1]. Of these coating layers, SiC is the main diffusion barrier to fission products (FPs). Hence, the modern fission nuclear reactor's safety and failure are dependent mostly on the integrity and the ability of the coating layers to contain all FPs [2].

Even with some improved performance some reports have indicated the inability of the coated particle to retain some radioactive FPs such as ^{110m}Ag during operation [1,2]. ^{110m}Ag is the product of a stable ^{109}Ag capturing a neutron. Although ^{109}Ag has a low fission yield (0.03% for 235U) and a conversion rate of 0.1%, the high gamma-rays dose rate of ^{110m}Ag and long half-life (about 253 days) are the concerns [3,4]. During the fission process in the fuel kernel, various FPs are produced concurrently with helium (He) from the alpha-decay of actinide elements (by neutron capture) and neutronic transmutation [5]. He forms bubbles in SiC [6]. The formation of bubbles may result in detrimental

* Corresponding author.
E-mail address: u14254744@tuks.co.za (S.Z. Mtsi).

https://doi.org/10.1016/j.vacuum.2023.112621
Received 7 June 2023; Received in revised form 13 September 2023; Accepted 14 September 2023
Available online 17 September 2023

effects on the integrity of SiC as the main diffusion barrier [7]. This compromise in integrity might result in SiC losing its legitimacy as the main diffusion barrier of fission products.

Owing to danger caused by the release of ^{110m}Ag, immense research has been done to thoroughly understand how silver is transported in SiC. These included in pile [4,8–10] and ion implantations [11–15]. Out of all the reported previous studies, only Hlatshwayo et al. investigated the effect of He bubbles in the migration of Ag into SiC [15]. In this previous work, 360 keV Ag ions were implanted into polycrystalline SiC to a fluence of 2×10^{16} cm^{-2} at room temperature (RT), then some of the Ag implanted samples were implanted with 17 keV He ions to a fluence of 1×10^{17} cm^{-2} also at RT. The Ag implanted and Ag and He co-implanted samples were annealed at 1100 °C for 5 h. Implantations at RT amorphized the crystal structure of SiC, while co-implantation of He resulted in the formation of nano-He bubbles in the amorphous layer. Annealing at 1100 °C resulted in the migration of Ag in the co-implanted annealed sample, indicating that He bubbles enhances the migration of Ag in the RT-implantation. However, to get more insight into how He influences the migration of Ag, similar investigations need to be performed in the He and Ag co-implanted SiC at elevated temperature to mimic the nuclear fission reactor environment. Hence, in this work, we investigated the synergistic effect of co-implantation of helium and silver into SiC at 350 °C by considering the structural evolution of SiC and the resulting migration behaviour of silver. To avoid bias and to establish correlation, we compared the current study with the previous results [15].

2. Experimental procedure

The base material utilized in this study was CVD-grown polycrystalline SiC wafers bought from Valley Design Corporation. Their lattice structures were predominantly cubic with some hexagonal growth modes present [11]. The implantation procedure used in this study are similar to one reported in Ref. [15]. However, in the current study both Ag and He implantations were done at an implantation temperature of 350 °C. Similar to the previous work, the Ag individually implanted SiC(Ag-SiC) and the Ag and He co-implanted SiC (Ag + He-SiC) samples were vacuum (10^{-5} Pa) annealed at 1100 °C for 5 h using a computer-controlled Webb 77 graphite furnace.

The Ag-SiC and Ag + He-SiC samples before and after annealing were characterized by Raman spectroscopy for microstructural changes, scanning electron microscopy (SEM) and atomic force microscopy (AFM) for morphological changes. Rutherford backscattering spectrometry (RBS) was used to monitor the implanted species. Additionally, the Ag + He-SiC samples were further characterized by transmission electron microscopy (TEM). A detailed procedure of Raman spectroscopy, TEM and TEM lamellae preparation can be found in RT study [15]. SEM micrographs were obtained using the Zeiss Ultra 55 field emission gun scanning electron microscopy (FEG-SEM). An in-lens detector was used to collect the signal and an accelerating voltage of 2 kV was applied. The surface morphology of Ag + He-SiC samples before and after annealing were also characterized using the Dimension Icon AFM system in contact mode. The AFM micrographs were analyzed using the Nano-Scope Analysis software over the scan area of 20 μm × 20 μm. Rutherford backscattering spectrometry (RBS) analysis, performed at the iThemba TAMS Laboratory, was used to monitor the implanted Ag species in the as-implanted and the samples annealed at 1100 °C. The RBS measurements were performed using 2 MeV helium ($4He^{+}$) particles. The backscattered particles were detected by a surface barrier detector placed at a scattering angle of 150°. An integrated charge of ~500 nC was collected to ensure sufficient statistics.

3. Results and discussion

Fig. 1 shows the simulated relative atomic density of Ag (360 keV) and He (17 keV) implanted into SiC, together with their simulated

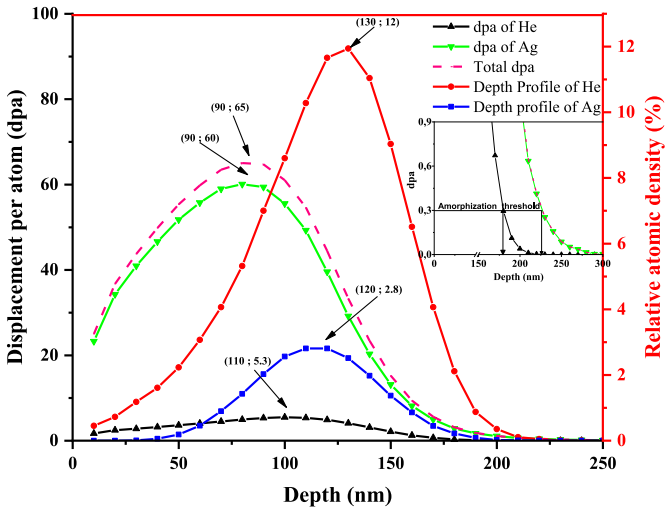

Fig. 1. SRIM-2013 simulation profiles of Ag (360 keV) ions and He (17 keV) ions implanted into SiC and the corresponding damage in displacement per atom (dpa) (Values in parentheses indicate the projected range and dpa of the ions relative to depth (nm)).

displacement per atom (dpa) as a function of depth in nm. Simulations were done using SRIM-2013 software [16]. Detailed calculations in full damage cascade mode and a SiC density of 3.21 g.cm^{-3} were used [17,18]. Carbon and silicon displacement energies of 20 eV and 35 eV, respectively, were adopted in the simulations [18,19]. The maximum concentrations of silver and helium are 3% and 12% at a projection range of 120 nm and 130 nm below the surface, respectively. As seen from Fig. 1, Ag and He have overlapping profiles, allowing the investigation of synergistic effects. The silver ions retain a maximum displacement of 60 dpa at a depth of 90 nm, while helium ions retain a maximum dpa of 5.3 at 110 nm below the surface. The total dpa (which is the sum of dpa retained by Ag and He ions) is 65 dpa at a depth of 90 nm below the surface. It is evident from simulated results that in both Ag-SiC and Ag + He-SiC the maximum retained dpa is above 0.3 dpa the assumed critical amorphization of SiC [20]. However, considering that the implantation temperature for both ions is 350 °C (which is above the critical amorphization temperature of about 300 °C), the SiC structure is not expected to be amorphized [20,21].

Fig. 2 shows the Raman spectra of the Ag-SiC and Ag + He-SiC samples before and after annealing. The Raman spectrum of the virgin SiC is included for comparison in Fig. 2. The Raman spectrum of virgin SiC has peaks at 799 cm^{-1} and 972 cm^{-1}, which correlate with the transverse (TO) and longitudinal (LO) phonon modes of cubic (3C-SiC). The TO mode shoulder at 772 cm^{-1} indicates the presence of some hexagonal (6H-SiC) polytype in the SiC layer [22]. Therefore, the polycrystalline SiC used in this work is predominantly contains 3C-SiC, with some traces of 6H-SiC structures present as was reported previously in Ref. [23]. Also visible in Fig. 2 are the transverse and longitudinal optical overtones at 1523 cm^{-1} and 1721 cm^{-1} [24]. Spectra of the as-implanted samples show a reduction in the intensity and broadening of the Raman characteristic peaks indicating accumulation of defects. Co-implantation resulted in the complete merging of TO mode peaks and the appearance of Si-Si and C-C peaks, indicating more defects in the co-implanted SiC [25]. The higher defect concentration in the co-implanted sample might be due to the interaction of defects produced by two successive implanted ions [23]. Although both individual and dual implantations resulted in significant damage to the crystal structure, the characteristic SiC peaks were still visible in both samples. Hence, complete amorphization was avoided owing to the high temperature of implantation (350 °C) that is above the critical amorphization temperature [21]. The thermal energy available during implantation increases the possibility for displaced atoms to combine

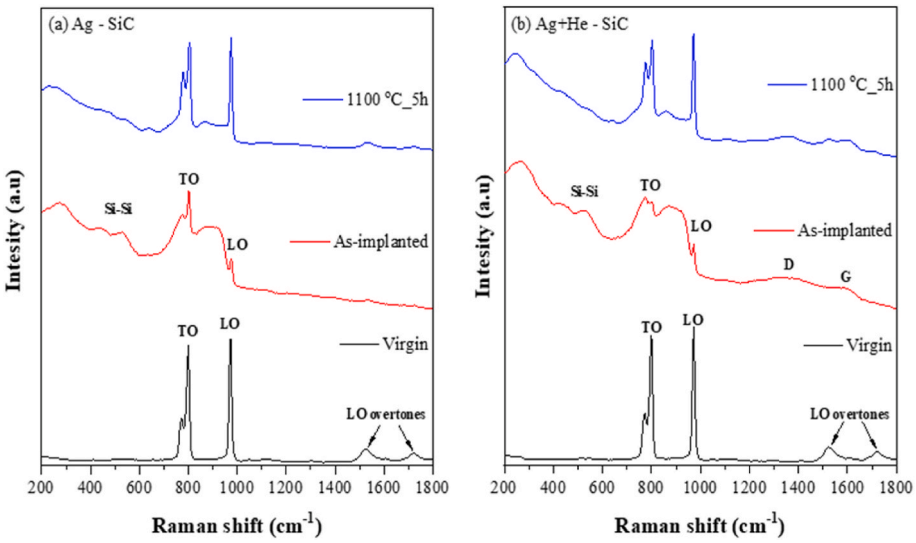

Fig. 2. The Raman spectra of Ag implanted SiC (a) and Ag & He co-implanted SiC (b) before and after annealing at 1100 °C for 5 h.

with vacancies. The appearance of the D and G carbon peaks in the co-implanted SiC Raman spectrum suggests that the presence of helium ions caused the graphitization of carbon in the SiC structure. Annealing of the as-implanted samples at 1100 °C caused the reappearance and increase in the intensity of the characteristic SiC peaks indicating healing or annealing out of defects. Annealing the co-implanted samples at 1100 °C also resulted in the D and G carbon peaks becoming more pronounced as compared to as-implanted Ag + He-SiC. This indicates further graphitization as a result of annealing. Graphitization of carbon is reported to restrict the recovery of the SiC crystal structure post-annealing in RT implantations [15]. In the samples implanted at a 350 °C graphitization of carbon also limited the recovery of the damaged SiC after annealing the co-implanted samples at 1100 °C.

Fig. 3 shows the SEM micrographs of Ag implanted samples before and after annealing. The surface of the virgin sample is flat with polishing marks as can be seen in Fig. 3(a). The polishing marks are due to polishing of hard surfaces during the manufacturing process [26]. The as-implanted micrograph (Fig. 3(b)) has fewer polishing marks on the surface. This is due to surface sputtering caused by the impact ions [24]. Less polishing marks also indicate swelling due to defects and lack of amorphization, correlating with Raman results [23]. Annealing the sample at 1100 °C resulted in the appearance of grains and their boundaries, as can be seen in Fig. 3(c). This indicates the recrystallization of the SiC implantation-damaged structure, which correlates with the Raman results.

Fig. 4 shows the SEM micrographs of the co-implanted samples before and after annealing at 1100 °C. The SEM micrograph of the Ag + He-SiC sample (Fig. 4(a)) has dark round structures and some bright

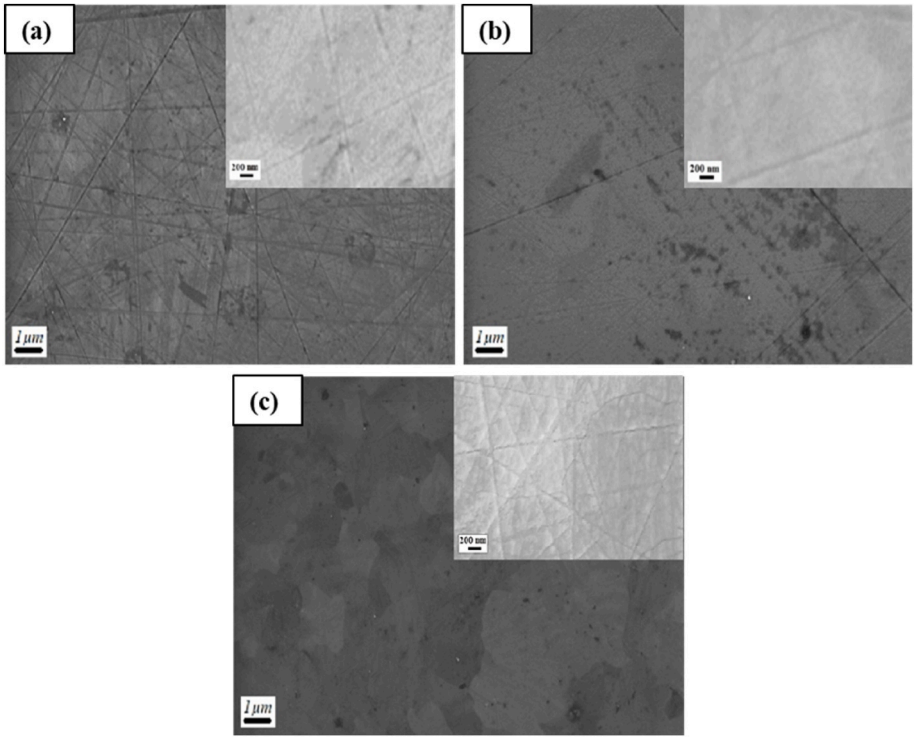

Fig. 3. SEM micrographs of the (a) virgin, (b) Ag implanted, and (c) annealed at 1100 °C for 5 h. The inserts are high magnification micrographs.

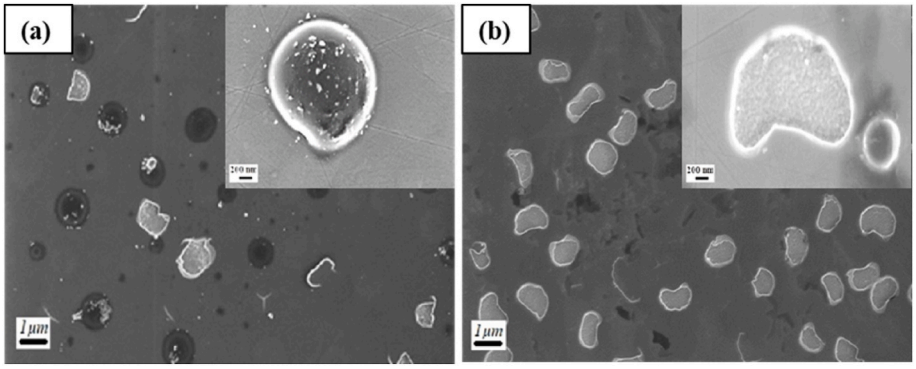

Fig. 4. SEM micrographs of the (a) Ag and He co-implanted, and (b) annealed at 1100 °C for 5 h. The inserts are high magnification micrographs.

irregular shape structures. These structures are uniformly distributed on the SiC surface. Annealing at 1100 °C increased the number of the bright structures, while dark structures seem to have disappeared. The structures found in the co-implanted SiC surface are due to helium implantation, as they are not present in Ag-only implanted samples (Fig. 3). The higher magnification in Fig. 4(a) suggests that dark spherical structures are protruding from the surface, and hence they can be assumed to be blisters caused by helium bubbles [27,28]. Consequently, the bright structures can also be presumed to be the holes resulting from the bursting of the blisters [29].

To further investigate whether these structures on the co-implanted samples are blisters and holes, AFM was used to analyse the surface topography of the co-implanted samples before and after annealing. Fig. 5 shows the AFM micrographs of the Ag + He-SiC before and annealed samples together with the profiles of the lines marked in the micrographs. All AFM micrographs show that SiC surfaces have bright and dark areas, correlating with SEM results (Fig. 4). The corresponding line profiles and scale bars indicate bright areas as topographical heights and dark-coloured as topographical depths. During the implantation of silver, energetic ions displaced atoms out of their lattice sites, resulting in vacancies and displaced atoms into the interstitial sites. When the He ions penetrate through the damage caused by the initial implantation (Ag ions), they increase the interstitials and vacancies densities. Helium's low probability to react with other atoms results to its trapping and clustering in vacancies [7]. Due to high-temperature implantations, free helium (in interstitials) diffuses into vacancies and agglomerates, forming He bubbles underneath the surface, thus creating (high--pressurized) He blisters on the surface [6,30], as seen in Fig. 5(a). Once blister reaches a critical size, due to pressure gradually increasing inside the bubble, it bursts and exfoliates the surface resulting in the formation of a hole [29,31]. Annealing at a temperature of 1100 °C resulted in more holes at the expense of blisters (Fig. 5(b)), which is consistent with the SEM micrographs of the co-implanted samples. Moreover, from Fig. S1(in supplementary data), it can be seen that after annealing, the area covered by holes increased from about 2% to about 8% while, the area covered by the blisters decreased from 22% to about 12% (note: the

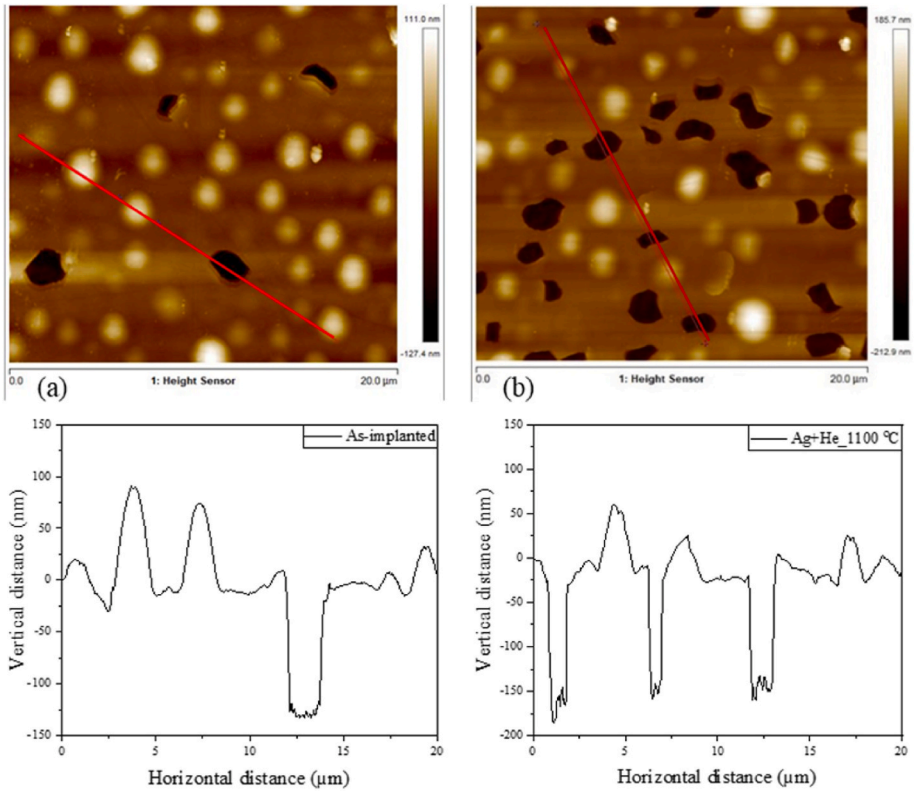

Fig. 5. AFM two-dimensional micrographs and line scans of the co-implanted SiC samples (a) before (as-implanted) and (b) after annealing at 1100 °C for 5 h.

surface areas of blisters and holes were calculated by assuming they were both perfect circular using *imageJ* program).

The migration of Ag in Ag-SiC and Ag + He-SiC samples before and after annealing at 1100 °C for 5 h was monitored using RBS analysis. Fig. 6 shows the RBS spectra of as-implanted and annealed Ag-SiC and Ag + He-SiC samples. The arrows indicate the surface channel positions of Ag, Si and C. The Ag depth profiles from RBS of the as implanted and annealed samples are shown in Fig. 7. The Ag depth profile of the as-implanted Ag-SiC sample has a projected range (Rp) at about 125 nm below the surface, which correlates with the SRIM simulated Rp estimate of 120 nm and is Gaussian and symmetric.

In this study, the squares of the full width at half maximum (FWHM) of the Ag depth profiles and retained ratio of Ag were calculated and they are plotted as a function of temperature as shown in Fig. 8. Co-implantation of He resulted in the slight broadening of Ag profile, indicating some limited diffusion of Ag. This was accompanied by the loss of about 7% of Ag from the surface indicating some limited-out diffusion and loss from the surface. This might be due to the presence of blisters and holes as discussed in the AFM results. The surface roughness is also known to contribute to broadening of the RBS profiles [32] while holes act as the out-migration paths. Annealing the Ag-SiC sample at 1100 °C caused some shift of Ag profile towards the bulk accompanied by neither broadening nor loss of implanted Ag indicating no detectable Fickian diffusion. The slight shift of Ag towards the bulk accompanied by neither broadening nor loss might be an indication of silver forming precipitates due to Ag segregating in the damaged SiC volume in the annealed Ag-SiC sample. Formation of Ag precipitates due to Ag segregating in the damaged SiC has been observed in Ag implanted into 6H-SiC at room temperature annealed firstly 900 °C for 10h and directly afterwards at 1250 °C for 30 min [1] and in the polycrystalline SiC co-implanted with Ag and Sr at 600 °C [23]. Annealing the Ag + He-SiC sample at 1100 °C resulted in a broadening of the Ag profile accompanied by a loss of about 22% indicating diffusion towards the surface and loss from the surface. This migration accompanied by loss might be due to more holes on the surface of the annealed Ag + He-SiC samples as seen in Fig. 5. Holes might also indicate the out-diffusion of He. The He depth profiles from heavy ions recoil detection analysis (ERDA) indicated some loss of He in the sample annealed at 1100 °C as shown in Fig. S2 (supplementary data). Moreover, the migration of Ag accompanied by loss occurred while the Ag peak position remained in the same position indicating some trapping of implanted Ag. Migration of Ag in the annealed Ag + He-SiC with no migration in the annealed Ag-SiC indicates that He bubbles somehow assist in the migration of implanted Ag.

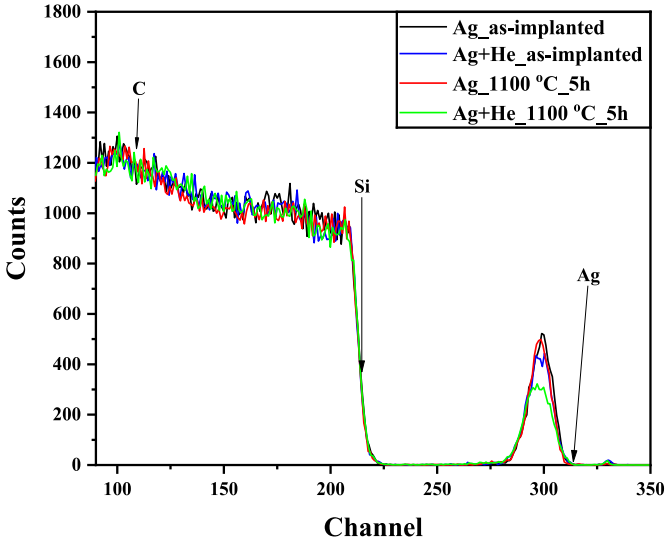

Fig. 6. RBS spectra of Ag-SiC and Ag + He-SiC as-implanted and annealed at 1100 °C for 5 h samples.

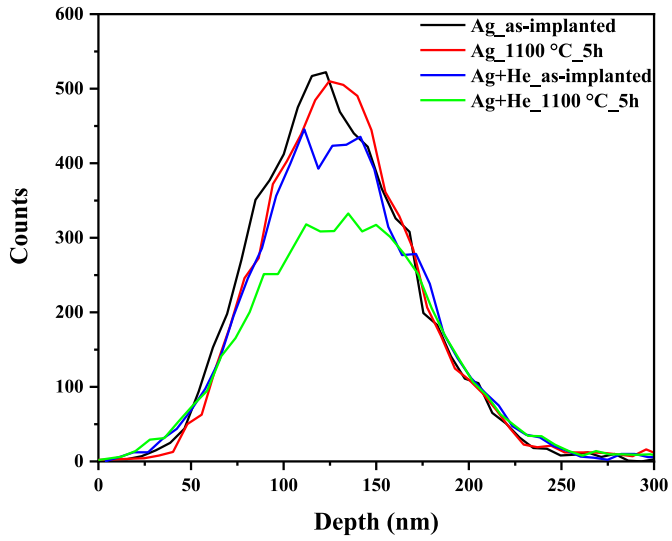

Fig. 7. The RBS depth profiles of Ag in Ag-SiC and Ag + He-SiC samples before and after annealing at 1100 °C for 5 h.

To get more insight into the migration of Ag in the Ag + He-SiC samples, the Ag + He-SiC samples were further characterized by TEM. Fig. 9 shows the cross-sectional bright-field (BF) TEM micrographs of the as-implanted and annealed Ag + He–SiC samples and their corresponding high magnification micrographs. The solid black line in Fig. 9 (a) indicates the damaged SiC (implanted region), while the blue double arrow indicates the bulk or undamaged SiC. Co-implantation of He in the Ag-SiC sample resulted in a total defective layer of about 233 nm from the surface thus most of implanted Ag is embedded on the defective SiC. In BF TEM micrographs, heavier elements appear darker because fewer electrons are transmitted while lighter elements appear brighter because more electrons are transmitted. Therefore, co-implantation of Ag and He resulted in the formation of larger elongated and smaller roundish bubbles from the 65–200 nm region below the surface (Fig. 9(a)). The agglomeration of helium in vacancies causes the formation of bubbles filled with helium underneath the surface [7,30]. Due to the high implantation temperature, some bubbles agglomerated resulting in an interconnected network or elongated He bubbles at about the projected range of implanted ions, as shown in the high magnification insert (Fig. 9(a')). Some dark regions are also observed in Fig. 9(a). These darker regions might be Ag rich regions indicating some Ag precipitates in the Ag + He-SiC sample. Ag precipitates have been observed in the Ag and Sr co-implanted at 600 °C with no Ag precipitates observed in the Ag only implanted SiC [23]. The formation of Ag precipitates at a lower implantation temperature in the current study might be due to He bubbles assisting the migration of Ag. Annealing caused the defective layer of about 30 nm from the surface (in the as-implanted Ag + He-SiC) to increase to about 73 nm. Owing to annealing, the 73 nm layer has less defects as can be seen in Fig. 9(b). These were accompanied by the transformation of elongated He bubbles into large and almost spherical He bubbles in the Ag + He-SiC annealed sample (Fig. 9(b ')), which resulted in an increase in the total damaged region to about 302 nm. This is due to the migration of vacancies and coalescence of bubbles resulting in larger bubbles during annealing [33]. Similar growth of He bubbles was reported for the He and Ag co-implanted into SiC at room temperature and annealed at 1100 °C for 5 h [15]. The growth of the He bubbles might also create defects (dislocation loops, stacking faults and strains) which can then increase the width of the damaged region [33]. More Ag-rich regions can be observed in the TEM micrograph of the annealed Ag + He-SiC (Fig. 9(b)), indicating that annealing resulted in the formation of more Ag precipitates.

EDX analysis was used to verify the chemical composition of the Ag

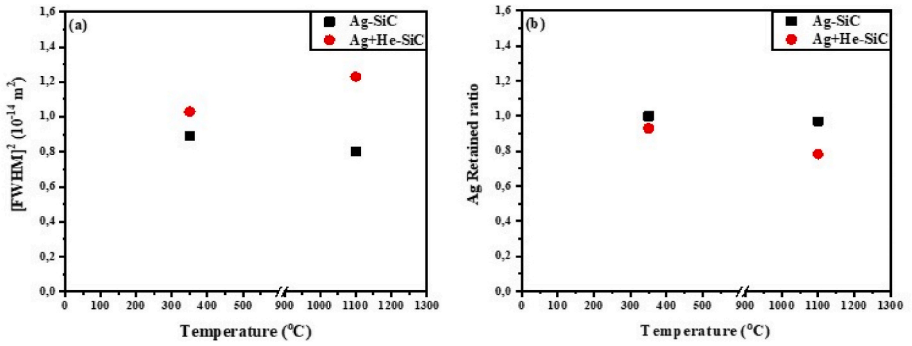

Fig. 8. (a) FWHM and (b) Retained ratio of Ag in Ag-SiC and Ag + He-SiC samples before and after annealing at 1100 °C for 5 h.

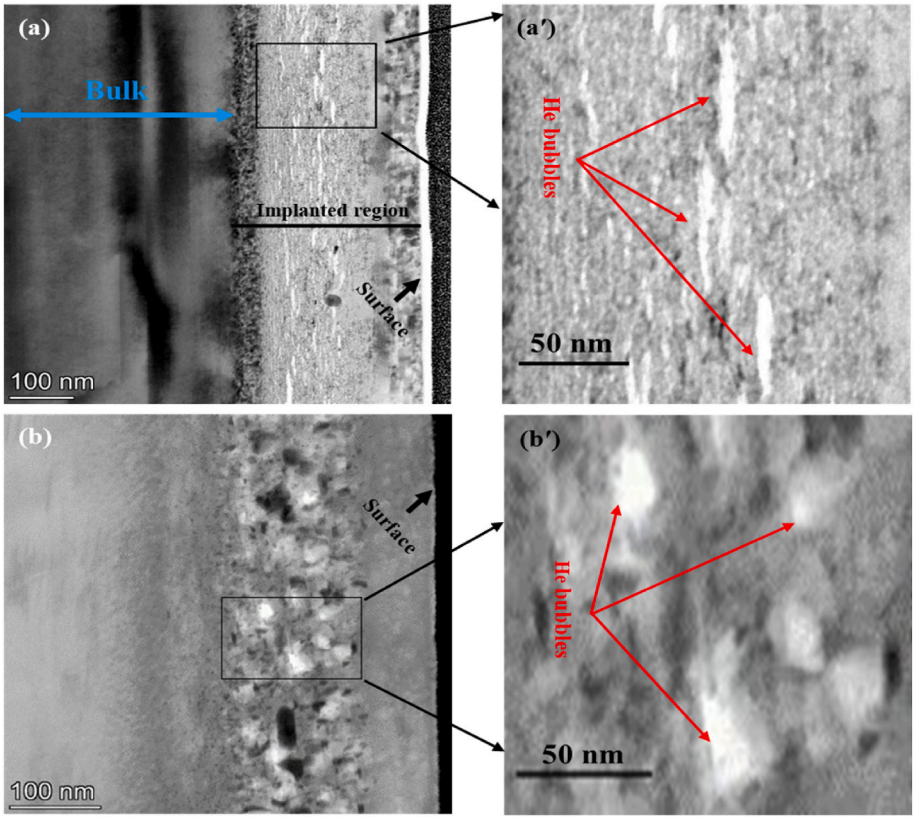

Fig. 9. Bright-field (BF) TEM micrographs of Ag + He-SiC (a) as-implanted and (b) annealed samples, with their corresponding high magnification inserts of the damaged region with He bubbles before (a') and (b') after annealing at 1100 °C.

+ He-SiC samples. Figs. 10 and 11 show the high-angle annular dark-field (HAADF) scanning transmission electron microscopy (STEM) micrographs and energy-dispersive X-ray (EDX) mappings of the as-implanted and annealed Ag + He-SiC samples. In HAADF inelastically scattered electrons (annulus around the beam) are used for imaging. Since heavier elements scatter more electrons they appear brighter in HAADF micrograph while lighter elements scatter few electrons and they appear darker [34]. Therefore, the bright regions within a red circle in Fig. 10(a) are the Ag precipitates. They were confirmed to be Ag precipitates, by the EDX mapping of Ag (Fig. 10(c)). The red circle in Fig. 10(d) shows the Si-deficient regions in the implanted layer where the He bubbles and Ag precipitates are formed and Fig. 10(b) shows that C is evenly distributed. The Ag precipitate (circled in red in Fig. 10(a) and (c)) formed in the same Si deficient region, as shown in Fig. 10(d). This implies that Ag precipitates might be trapped in cavities. The cavities are the results of He out-diffusion. Annealing at 1100 °C resulted in the formation of more Ag precipitates in the implanted region, which consequently led to more Si deficient regions, as shown in Fig. 11(a), (c) and (d). Ag precipitates are visibly brighter than the as-implanted ones, implying that more Ag is trapped in cavities. The Si-poor regions might also be due to the growth (in size) of He bubbles/cavities. Moreover, annealing also resulted in a slightly C-poor regions in the implanted region, as seen in Fig. 11(b) which is due to growth in Ag precipitates.

In this study, He ions were co-implanted into SiC with defects retained by implanted Ag and helium bubbles are formed when helium atoms capture vacancies/interstitials. These defects and the high helium implantation temperature resulted in the clustering of He-vacancy/interstitials thus the formation of bubbles in the highly defective regions of the as-implanted Ag + He-SiC which caused blisters on the surface. Depending on the amount of pressure in the bubbles, some of the blisters burst resulting in some out-diffusion of He and Ag along with the appearance of holes on the Ag + He-SiC surfaces. The out diffusion of He also resulted in cavities in the implanted SiC layer. Therefore, the migration of Ag in the as-implanted Ag + He-SiC samples is due to

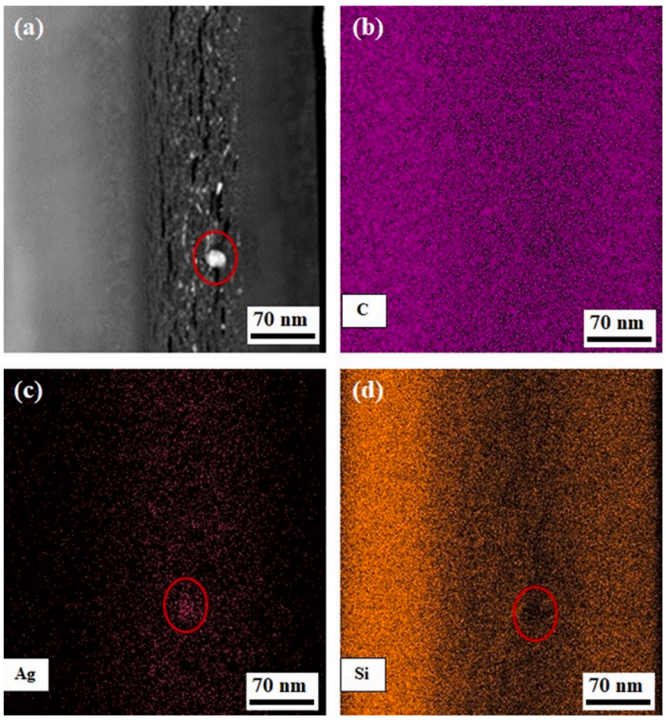

Fig. 10. (a) Cross-sectional HAADF STEM image of Ag + He co-implanted into polycrystalline SiC, and EDX elemental maps of b) C, c) Ag, d) Si.

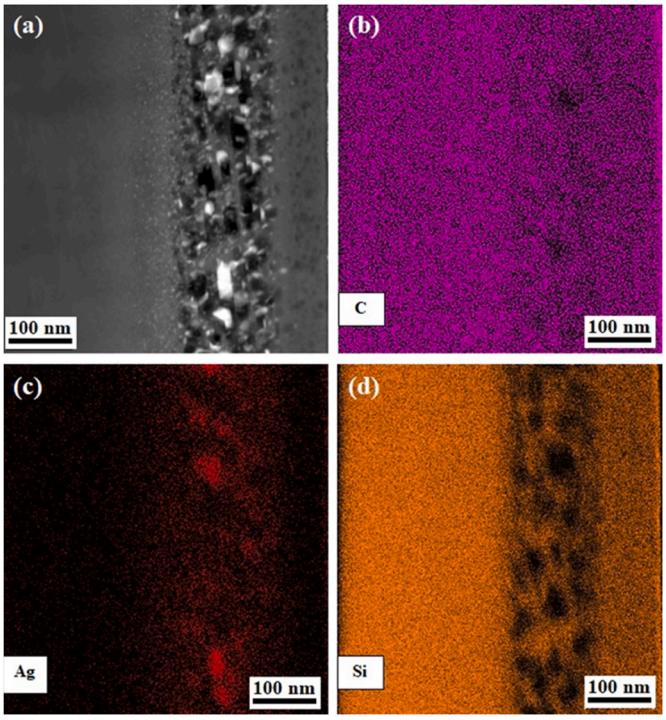

Fig. 11. (a) Cross-sectional HAADF STEM image of Ag + He co-implanted and annealed at 1100 °C for 5 h, and EDX elemental maps of (b) C, (c) Ag and (d) Si.

vacancy/interstitial diffusion during the formation of He bubbles. Moreover, some of the diffusing Ag was lost via the holes during implantation and some precipitated on the cavities in the implanted SiC layer. Annealing at 1100 °C caused the coalescence of more bubbles and some out-diffusion of He resulting in large bubbles, holes and cavities in the annealed Ag + He-SiC. During the coalescence of bubbles more Ag out diffused resulting in additional loss of Ag via holes and more Ag precipitates trapped in the cavities. The simulated, RBS and TEM results (Figs. 1, Figs. 7 and 9) further pointed out that the highly defective region where He bubbles are formed is the region with most of the implanted Ag. Thus, this region is also expected to have maximum strain due to implanted Ag [35]. For bubbles to grow in the highly defective region, they will have to capture vacancies/interstitials in the less defective regions (i.e. in the 30 nm layer before the highly defective and the one beyond the highly defective region), this will also allow the implanted Ag atoms to move in the opposite direction of the vacancies/interstitials, i.e., via vacancy diffusion or interstitial diffusion. Hence, the growth of He bubbles accompanied by migration towards the surface is due to either vacancy diffusion or interstitial diffusion driven by strain fields. The combination of both vacancy and interstitial diffusion is also possible in this system as it has been observed that the interstitials start to diffuse from low strained area to the highly strained area [35]. These results are in agreement with the results of Ag and He co-implanted into SiC at room temperature annealed at 1100 °C for 5 h [15]. However, the migration of Ag was more pronounced in the annealed RT co-implanted samples due to high concentration of defects in the amorphous SiC structure. These are important results for the application of SiC in modern fission reactor environments. However, more investigations need to be carried out especially at elevated temperatures to gain more insight into the understanding of the role of He in the migration of Ag.

4. Conclusion

In this work, the effects of He bubbles and annealing on the structural evolution and migration behavior of Ag implanted into polycrystalline SiC at 350 °C were investigated. 360 keV Ag ions were implanted into SiC to a fluence of 2×10^{16} cm^{-2} at 350 °C, on the same Ag implanted sample, 17 keV He ions were implanted to a fluence of 1×10^{17} cm^{-2} also at 350 °C. The Ag implanted and co-implanted samples were then annealed at a temperature of 1100 °C for 5 h. Both individual implantation and co-implantation accumulated defects in the SiC structure without amorphization. Moreover, co-implantation led to the formation of He bubbles around the projected range or the highly defective region of the implanted SiC layer. This was accompanied by the formation of blisters and some holes on the surface of SiC indicating He bubbles and some cavities within the implanted region. Annealing caused some recrystallization in both samples albeit more pronounced in the Ag implanted SiC sample. The limited recrystallization in the co-implanted samples was caused by the appearance of larger bubbles and cavities in the annealed implanted region of the co-implanted samples. Migration of Ag resulting in the formation of Ag precipitates in cavities and loss were observed in the as-implanted co-implanted samples indicating that He bubbles assist in the migration of Ag. Further migration accompanied by the formation of larger Ag precipitates trapped in cavities and loss of implanted Ag were observed in the co-implanted samples annealed at 1100 °C. No migration was observed in the Ag implanted samples annealed at 1100 °C. Hence, He bubbles assist the migration of Ag while cavities trap Ag in SiC. The Ag migration mechanism was explained in terms of vacancy/interstitial diffusion assisted by strain gradient. The findings of this study have far-reaching implications for the application of SiC in nuclear reactor environments. Although, more investigations need to be conducted at elevated temperatures and atomic level to understand the role of He in Ag migration.

CRediT authorship contribution statement

S.Z. Mtsi: Writing – original draft, Visualization, Investigation, Formal analysis, Conceptualization. **A. Sohatsky:** Validation, Resources. **Z.A.Y. Abdalla:** Writing – review & editing, Investigation. **E.G. Njoroge:** Validation, Investigation. **V.A. Skuratov:** Validation, Investigation. **S.V. Motloung:** Validation. **J.B. Malherbe:** Validation, Resources. **T.T. Hlatshwayo:** Writing – review & editing, Supervision,

Resources.

Declaration of competing interest

The authors declare that they have no known competing financial interests or personal relationships that could have appeared to influence the work reported in this paper.

Data availability

Data will be made available on request.

Acknowledgements

Financial support by the National Research Foundation of South Africa (Grant numbers: 142104, 120471 and 2204072593) is gratefully acknowledged.

Appendix A. Supplementary data

Supplementary data to this article can be found online at https://doi.org/10.1016/j.vacuum.2023.112621.

References

[1] J.B. Malherbe, Diffusion of fission products and radiation damage in SiC, J. Phys. Appl. Phys. 46 (47) (2013), 473001.
[2] P.A. Demkowicz, B. Liu, J.D. Hunn, Coated particle fuel: historical perspectives and current progress, J. Nucl. Mater. 515 (2019) 434–450.
[3] E. Friedland, N.G. Van Der Berg, J.B. Malherbe, J.J. Hancke, J. Barry, E. Wendler, W. Wesch, Investigation of silver and iodine transport through silicon carbide layers prepared for nuclear fuel element cladding, J. Nucl. Mater. 410 (1–3) (2011) 24–31.
[4] P.E. Brown, R.L. Faircloth, Metal fission product behaviour in high temperature reactors-UO2 coated particle fuel, J. Nucl. Mater. 59 (1) (1976) 29–41.
[5] M.R. Gilbert, J.C. Sublet, Neutron-induced transmutation effects in W and W-alloys in a fusion environment, Nucl. Fusion 51 (4) (2011), 043005.
[6] M.F. Beaufort, M. Vallet, J. Nicola, E. Oliviero, J.F. Barbot, In-situ evolution of helium bubbles in SiC under irradiation, J. Appl. Phys. 118 (20) (2015), 205904.
[7] L. Yang, X.T. Zu, H.Y. Xiao, F. Gao, H.L. Heinisch, R.J. Kurtz, Defect production and formation of helium–vacancy clusters due to cascades in α-iron, Phys. B Condens. Matter 391 (1) (2007) 179–185.
[8] H. Nabielek, P.E. Brown, P. Offermann, Silver release from coated particle fuel, Nucl. Technol. 35 (2) (1977) 483–493.
[9] R.E. Bullock, Fission-product release during postirradiation annealing of several types of coated fuel particles, J. Nucl. Mater. 125 (3) (1984) 304–319.
[10] J.J. Van der Merwe, Evaluation of silver transport through SiC during the German HTR fuel program, J. Nucl. Mater. 395 (1–3) (2009) 99–111.
[11] E. Friedland, J.B. Malherbe, N.G. van der Berg, T.T. Hlatshwayo, A.J. Botha, E. Wendler, W. Wesch, Study of Silver diffusion in silicon carbide, J. Nucl. Mater. 389 (2) (2009) 326–331.
[12] T.T. Hlatshwayo, J.B. Malherbe, N.G. Van Der Berg, A.J. Botha, P. Chakraborty, Effect of thermal annealing and neutron irradiation in 6H-SiC implanted with silver at 350 °C and 600 °C, Nucl. Instrum. Methods Phys. Res. Sect. B Beam Interact. Mater. Atoms 273 (2012) 61–64.
[13] T.T. Hlatshwayo, J.B. Malherbe, N.G. Van Der Berg, L.C. Prinsloo, A.J. Botha, E. Wendler, W. Wesch, Annealing of silver implanted 6H–SiC and the diffusion of the silver, Nucl. Instrum. Methods Phys. Res. Sect. B Beam Interact. Mater. Atoms 274 (2012) 120–125.
[14] H.A.A. Abdelbagi, V.A. Skuratov, S.V. Motloung, E.G. Njoroge, M. Mlambo, J. B. Malherbe, J.H. O'Connell, T.T. Hlatshwayo, Effect of swift heavy ions irradiation in the migration of silver implanted into polycrystalline SiC, Nucl. Instrum. Methods Phys. Res. Sect. B Beam Interact. Mater. Atoms 461 (2019) 201–209.
[15] T.T. Hlatshwayo, C.E. Maepa, M. Msimanga, M. Mlambo, E.G. Njoroge, V. A. Skuratov, S.V. Motloung, J.B. Malherbe, Helium assisted migration of silver implanted into SiC, Vacuum 183 (2021), 109865.
[16] J.F. Ziegler, M.D. Ziegler, J.P. Biersack, SRIM–The stopping and range of ions in matter (2010), Nucl. Instrum. Methods Phys. Res. Sect. B Beam Interact. Mater. Atoms 268 (11–12) (2010) 1818–1823.
[17] U. Saha, K. Devan, S. Ganesan, A study to compute integrated dpa for neutron and ion irradiation environments using SRIM-2013, J. Nucl. Mater. 503 (2018) 30–41.
[18] W.J. Weber, F. Gao, R. Devanathan, W. Jiang, The efficiency of damage production in silicon carbide, Nucl. Instrum. Methods Phys. Res. Sect. B Beam Interact. Mater. Atoms 218 (2004) 68–73.
[19] R. Devanathan, W.J. Weber, Displacement energy surface in 3C and 6H SiC, J. Nucl. Mater. 278 (2000) 258–265.
[20] C.J. McHargue, J.M. Williams, Ion implantation effects in silicon carbide, Nucl. Instrum. Methods Phys. Res. Sect. B Beam Interact. Mater. Atoms 80 (1993) 889–894.
[21] W.J. Weber, L.M. Wang, N. Yu, N.J. Hess, Structure and properties of ion-beam-modified (6H) silicon carbide, Mater. Sci. Eng. 253 (1–2) (1998) 62–70.
[22] J. Wasyluk, T.S. Perova, S.A. Kukushkin, A.V. Osipov, N.A. Feoktistov, S. A. Grudinkin, Raman investigation of different polytypes in SiC thin films grown by solid-gas phase epitaxy on Si (111) and 6H-SiC substrates, Mater. Sci. Forum 645 (2010) 359–362.
[23] T.T. Hlatshwayo, N. Mtshonisi, E.G. Njoroge, M. Mlambo, M. Msimanga, V. A. Skuratov, J.B. Malherbe, S.V. Motloung, Effect of Ag and Sr dual implanted into SiC, Nucl. Instrum. Methods Phys. Res., Sect. B 472 (2020) 7–13.
[24] Z.A.Y. Abdalla, M.Y.A. Ismail, E.G. Njoroge, T.T. Hlatshwayo, E. Wendler, J. B. Malherbe, Migration behaviour of selenium implanted into polycrystalline 3C-SiC, Vacuum 175 (2020), 109235.
[25] M.J. Madito, T.T. Hlatshwayo, C.B. Mtshali, Chemical disorder of a-SiC layer induced in 6H-SiC by Cs and I ions co-implantation: Raman spectroscopy analysis, Appl. Surf. Sci. 538 (2021), 148099.
[26] J.B. Malherbe, N.G. van der Berg, A.J. Botha, E. Friedland, T.T. Hlatshwayo, R. J. Kuhudzai, E. Wendler, W. Wesch, P. Chakraborty, E.F. Da Silveira, SEM analysis of ion implanted SiC, Nucl. Instrum. Methods Phys. Res. Sect. B Beam Interact. Mater. Atoms 315 (2013) 136–141.
[27] N. Daghbouj, J. Lin, H.S. Sen, M. Callisti, B. Li, M. Karlik, T. Polcar, Z. Shen, M. Zhou, T. You, X. Ou, Blister formation in He-H co-implanted InP: a comprehensive atomistic study, Appl. Surf. Sci. 552 (2021), 149426.
[28] B.S. Li, Z.G. Wang, H.P. Zhang, Study of surface blistering in GaN by hydrogen implantation at elevated temperatures, Thin Solid Films 590 (2015) 64–70.
[29] N. Daghbouj, B.S. Li, M. Karlik, A.J.A.S.S. Declemy, 6H-SiC blistering efficiency as a function of the hydrogen implantation fluence, Appl. Surf. Sci. 466 (2019) 141–150.
[30] T. Mokgadi, Z. Abdalla, H. Abdelbagi, M. Msimanga, C. Maepa, V. Skuratov, T. Hlatshwayo, Helium and strontium co-implantation into SiC at room temperature and isochronal annealing: structural evolution of SiC and migration behaviour of strontium, Mater. Chem. Phys. 294 (2022), 126998.
[31] Q. Shen, G. Ran, W. Zhou, C. Ye, Q. Feng, N. Li, Investigation of surface morphology of 6H-SiC irradiated with He^{+} and H^{2+} ions, Materials 11 (2) (2018) 282.
[32] H. Metzner, T. Hahn, M. Gossla, J. Conrad, J.H. Bremer, Rutherford backscattering spectroscopy of rough films: experimental aspects, Nucl. Instrum. Methods Phys. Res. Sect. B Beam Interact. Mater. Atoms 134 (2) (1998) 249–261.
[33] B.S. Li, H.S. Sen, N. Daghbouj, A.T. AlMotasem, J. Lorinčík, M. Karlik, F.F. Ge, L. Zhang, Z. Sofer, I. Elantyev, M. Callisti, Thermal behavior of iron in 6H-SiC: influence of He-induced defects, Scripta Mater. 218 (2022), 114805.
[34] P.D. Nellist, S.J. Pennycook, The principles and interpretation of annular dark-field Z-contrast imaging, Adv. Imag. Electron. Phys. 113 (2000) 147–203.
[35] S. Leclerc, M.F. Beaufort, A. Declémy, J.F. Barbot, Strain-induced drift of interstitial atoms in SiC implanted with helium ions at elevated temperature, J. Nucl. Mater. 397 (2010) 132–134.